



Hyperspectral analysis for standoff detection of dimethyl methylphosphonate on building materials



Daniel Baseley^a, Luke Wunderlich^b, Grady Phillips^c, Kevin Gross^c, Glen Perram^c, Stuart Willison^d, Rebecca Phillips^d, Matthew Magnuson^d, Sang Don Lee^d, Willie F. Harper Jr.^{a,*}

^a Air Force Institute of Technology, Department of Systems Engineering and Management, 2950 Hobson Way, Wright-Patterson AFB, OH 45433, USA

^b Wright State University, Department of Biomedical Engineering, Dayton, OH 45435, USA

^c Air Force Institute of Technology, Department of Engineering Physics, 2950 Hobson Way, Wright-Patterson AFB, OH 45433, USA

^d US Environmental Protection Agency, National Homeland Security Research Center, 26 W. Martin Luther King Dr., Mailstop NG-16, Cincinnati, OH 45268, USA

ARTICLE INFO

Article history:

Received 1 April 2016

Received in revised form

15 August 2016

Accepted 27 August 2016

Available online 29 August 2016

Keywords:

Hyperspectral imaging

Organophosphate

Contrast angle

Surface analysis

Decontamination

ABSTRACT

Detecting organophosphates in indoor settings can greatly benefit from more efficient and faster methods of surveying large surface areas than conventional approaches, which sample small surface areas followed by extraction and analysis. This study examined a standoff detection technique utilizing hyperspectral imaging for analysis of building materials in near-real time. In this proof-of-concept study, dimethyl methylphosphonate (DMMP) was applied to stainless steel and laminate coupons and spectra were collected during active illumination. Absorbance bands at approximately 1275 cm^{-1} and 1050 cm^{-1} were associated with phosphorus-oxygen double bond (P=O) and phosphorus-oxygen-carbon (P–O–C) bond stretches of DMMP, respectively. The magnitude of these bands increased linearly ($r^2 = 0.93$) with DMMP across the full absorbance spectrum, between $\nu_1 = 877\text{ cm}^{-1}$ to $\nu_2 = 1262\text{ cm}^{-1}$. Comparisons between bare and contaminated surfaces on stainless steel using the spectral contrast angle technique indicated that the bare samples showed no sign of contamination, with large uniformly distributed contrast angles of 45° – 55° , while the contaminated samples had smaller spectral contact angles of $<20^\circ$ in the contaminated region and $>40^\circ$ in the uncontaminated region. The laminate contaminated region exhibited contact angles of $<25^\circ$. To the best of our knowledge, this is the first report to demonstrate that hyperspectral imaging can be used to detect DMMP on building materials, with detection levels similar to concentrations expected for some organophosphate deposition scenarios.

Published by Elsevier Ltd.

1. Introduction

Monitoring the indoor environment is an important priority because people spend large portions of time inside of buildings [24,26]. Indoor monitoring has been carried out for a wide range of conditions and air pollutants [7,9,13,21,29], and there is now a need to expand these efforts to address rising concerns related to the presence of organophosphate (OP) compounds on indoor surfaces. This may be caused by over-application of pesticides in homes, and in some cases by incidental transport from residential areas (e.g. gardens, playgrounds) or outdoor workplaces where pesticide

application is heavy [5]. Indoor OP exposure may also result from intentional or accidental release of compounds used as chemical warfare agents. There have been previous efforts to detect OPs on indoor surfaces [30]. OPs have been previously linked to leukemia [6,17], prostate cancer [2], Non-Hodgkin's lymphoma [6], and pediatric mental disorders such as pediatric attention-deficit/hyperactivity disorder (ADHD) [17]. Thus, severe public health consequences can result from OP exposure.

Decontamination of indoor surfaces would be greatly aided by fast and accurate screening and detection methods for OPs. Currently, OPs are often detected via chromatographic methods, which are expensive and require extensive sample preparation and laboratory analysis. Further, the current sampling collection methods rely on labor intensive surface wipe sampling. This limits the total number of samples that can be collected and increases the

* Corresponding author.

E-mail address: willie.harper@afit.edu (W.F. Harper).

possibility that some contamination may go undetected. Shipping, handling, and processing of the number of samples generated from a contaminated area will also create a backlog during sample preparation and analysis, thus, delaying decontamination efforts and decision-making during the remediation phase of an incident. A standoff detection method, via use of field instrumentation, would be an effective tool to reduce the working time (i.e., time needed to survey, sample, analyze, and detect target analytes in an area) by fast screening large areas for potential OP contamination, identifying hot spots (as well as areas where contamination may not be present), allowing workers to decontaminate the surfaces immediately, enabling monitoring of the decontamination progress, and reducing sample load on the laboratory.

Optical imaging methods employing ultraviolet absorption or use of fluorophores have been reported for chemical detection (e.g. Refs. [18,27]). Optical spectroscopy, in particular, takes advantage of characteristic vibrational frequencies in the optical spectra for detecting various molecules [16]. used a high spatial resolution hyperspectral imaging system to reveal a chlorophyll absorption waveband (685 nm) and two bands in the near infra-red region to identify apples that were contaminated with soil or fungus. Similar work has been investigated for the detection of contaminated fruit [10,14] and the detection of fecal coliforms on poultry carcasses [12]. Hyperspectral imaging techniques have also been used to detect prostate cancer [1], damaged tooth enamel [23], and to detect water stress in plants [11]. Environmental monitoring can also benefit from using hyperspectral imaging techniques. A recent example from Ref. [4]; presents preliminary data which distinguished both VX (IUPAC name O-ethyl S-[2-(diisopropylamino) ethyl] methylphosphonothioate) and sulfur mustard from benign compounds using mid-wave infrared hyperspectral imaging. Thus, hyperspectral imaging, a technique well-established in other technical fields, may be a viable standoff approach for OP detection on indoor surfaces.

This study investigates the ability of hyperspectral imaging to detect OPs on common indoor building materials. Data processing approaches enabling qualitative and quantitative detection will be developed to demonstrate the proof-of-concept for this approach. This study utilized dimethyl methyl phosphonate (DMMP) as a surrogate for common organophosphate pesticides and structurally related chemical warfare agents.

2. Materials and methods

2.1. Equipment and materials

2.1.1. Hyperspectral imager

The instrument used for this investigation was a Telops Hyper-Cam (Telops Inc., Quebec City, Quebec, Canada) which is composed of a long-wave infrared (LWIR, 8–12 μm) imaging Fourier Transform Spectrometer, LW-IFTS, as shown in Fig. 1a. The LW-IFTS is described previously in Ref. [15]. A 320×256 pixel (30 μm pixel pitch) HgCdTe focal plan array (FPA) is integrated with a Michelson interferometer. A series of modulated intensity images corresponding to various optical path differences were collected on the FPA, forming a double-sided interferogram at each pixel. A Fourier transform of each pixel's interferogram produces an uncalibrated spectrum. Two internal blackbody sources at 25 and 50 $^{\circ}\text{C}$ were used to calibrate the instrument for absolute spectral radiance [20]. The interferometer has a native spectral resolution of 0.25 cm^{-1} , but this was degraded to 4 cm^{-1} in order to improve the signal-to-noise ratio. The spectral bandwidth is limited to $833\text{--}1250 \text{ cm}^{-1}$ by the HgCdTe detector. The instantaneous field of view using an f/2 collection optic is 0.8 mm/pixel. Temporal averaging was used for 20–40 hyperspectral data cubes to improve the signal

to noise ratio. Typical signals at zero optical path difference were $10 \mu\text{W}/\text{cm}^2 \text{ sr cm}^{-1}$, or 25% of the camera's 16 bit dynamic range. The 1σ variance in the spectral radiance was typically $\sim 0.002 \mu\text{W}/\text{cm}^2 \text{ sr cm}^{-1}$.

2.1.2. Building material coupon preparation

Building materials included 4" x 4" coupons made of polished stainless steel (McMaster Carr, Elmhurst, IL) or laminate (Home Depot, Cincinnati, OH). DMMP (Alpha Aesar, Ward Hill, MA) was applied to a portion of the coupon yielding surface densities of $22 \mu\text{g}/\text{cm}^2 - 1.1 \text{ mg}/\text{cm}^2$. The following materials were chosen because they will likely result in minimal target analyte loss into the material due to absorption, yet, still are common materials found within an urban setting. Several application methods were used. First, 10, 25 or 50 μL droplet of a 98% DMMP solution was applied to the surface and then smeared with the tip of a pipette. An additional method included applying 1, 5 and 10 μL volumes of 98% DMMP solution with methanol in a 1:1 ratio to the surface, covering half the coupon surface, then allowing the methanol to evaporate. Finally, a 10 μL of DMMP was applied in an "X" pattern in the center of the coupon.

2.2. Data collection

Contaminated surfaces were illuminated with an extended-area blackbody (Electro Optic Industries, Inc., Model CE600-06, Santa Barbara, CA, USA) and imaged by the LW-IFTS instrument as shown in Fig. 1b. Emissions from infrared sources may be attenuated by two passing through the contaminated film, reflecting off of the metal surface, and passing back through the film toward the imager. Alternatively, the source may preferentially heat the contaminant, leading to a positive temperature difference with the surface and an emission spectrum. The building material coupons were held vertically in a lab hood at a 45° angle relative to the face of the hood. The blackbody illumination source was placed inside the hood, facing the sample at a 45° angle. The Telops Hyper-cam was set up outside of the lab hood, also at a 45° angle to the surface. For each image collected, an equal number of acquisitions for each blackbody were also collected for calibration purposes. Once the sample was in place, the temperature of the illumination blackbody was adjusted so the signal in the contaminated area was between that of the two internal blackbodies.

3. Results

3.1. The effect of DMMP on spectral radiance

Typical spectra for DMMP on both stainless steel and laminate are provided in Fig. 2. These spectra were spatially averaged over the center of the image. The blackbody signal for the stainless steel surface was increasingly attenuated as the quantity of DMMP applied increased. The signal can be converted to absorbance,

$$A(\nu) = -\ln\left(\frac{I(\nu)}{I_0(\nu)}\right) \cong \frac{I_0(\nu) - I(\nu)}{I_0(\nu)} \quad (1)$$

where I_0 = spectral intensity of the bare sample, and I = spectral intensity of the contaminated surface, as shown in Fig. 3a. The absorbance values for the stainless steel samples were low and can be approximated by the fractional difference between the sample and bare sample. The observed spectra were well correlated with a standard reference absorption spectrum for liquid DMMP [19,22]. Absorbance bands at approximately 1275 cm^{-1} and 1050 cm^{-1} were associated with the phosphorus-oxygen double bond (P=O) and phosphorus-oxygen-carbon (P-O-C) bond stretches of DMMP,

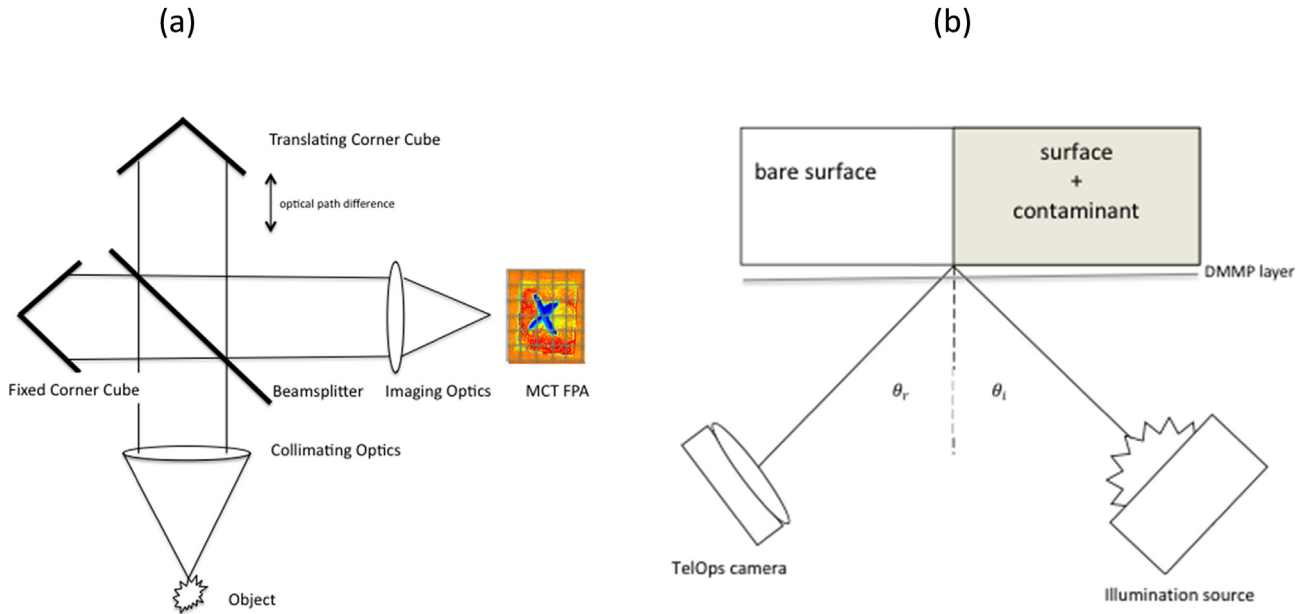


Fig. 1. (a) LW-IFTS hyperspectral sensor and (b) experimental layout.

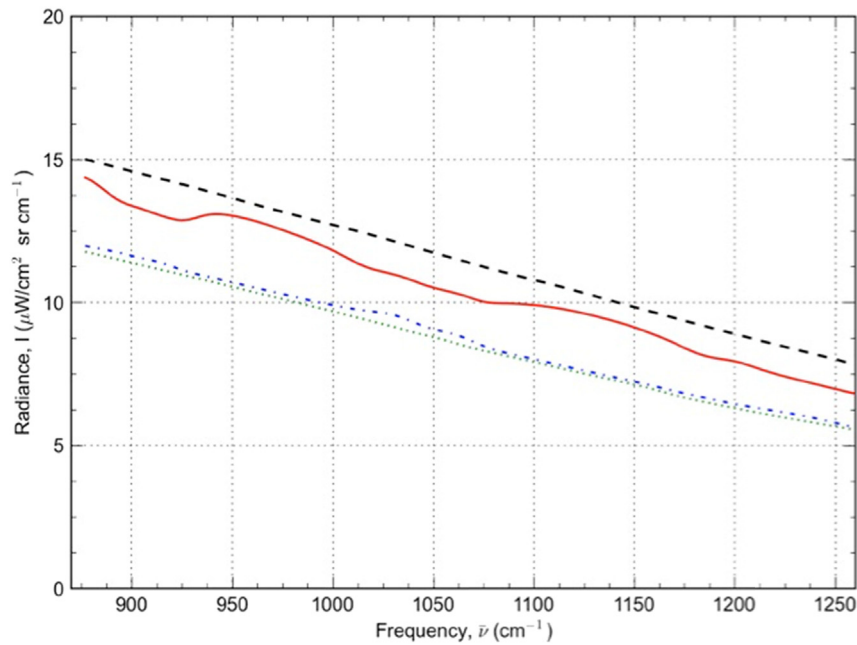


Fig. 2. Calibrated spectral radiance for 50 μL DMMP on: (—) stainless steel and (-.-.-) laminate. The spectra for (---) bare stainless steel is somewhat larger than for (.....) bare laminate due to higher reflectivity.

respectively [3,28]. The feature shown at 1050 cm^{-1} can be seen on Fig. 3a and b, however the 1275 cm^{-1} feature is only partially visible due to the wavenumber range.

The spectral radiance for DMMP on laminate (Fig. 2) was larger than the bare material. This may occur because the laminate was heated by higher surface absorption and had lower thermal conductivity relative to the polished metal. This may have led to a contaminant layer that was slightly warmer than the surface and a net emission from the DMMP. The absorbance bands and relative amplitudes were slightly shifted relative to the stainless steel surface. These shifts may have been caused by: (1) the key functional groups forming chemical bonds with the surface material, (2) the

chemical application changing the mechanical properties of the underlying material, or (3) non-uniform film thickness. It seemed more likely that a change in film thickness contributed to the observed shifts. In general, the location of the absorbance bands for P=O and P-O-C bond stretches depended on the nature of the building material and the thickness of the chemical layer [3,28]. The increase in spectral radiance over the bare material was further characterized for several contamination levels in Fig. 3b, which presents the data as enhanced intensity as opposed to absorbance (this format avoids showing negative absorbance and facilitates comparison to Fig. 3a). For both laminate and SS, the differences between the measured profiles and the reference profiles increased

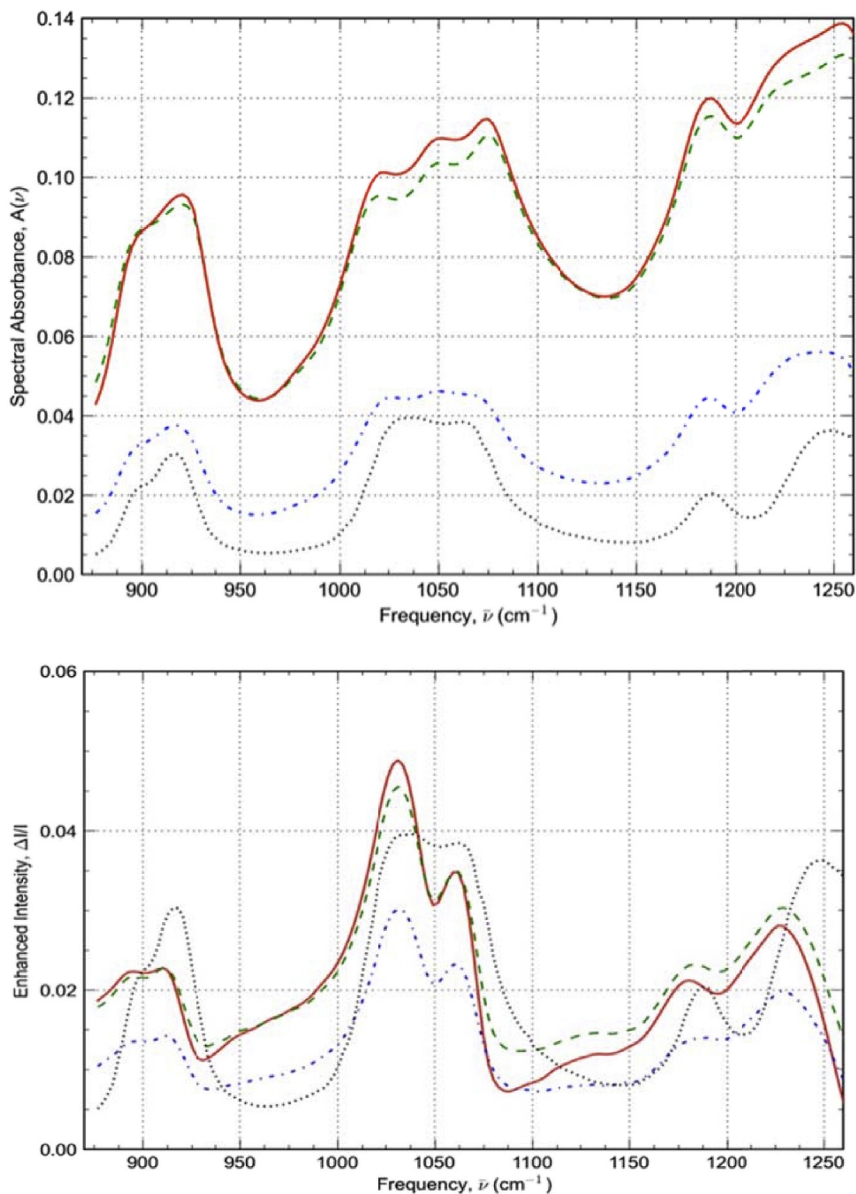


Fig. 3. (a-top) Absorbance for DMMP on stainless steel and (b-bottom) enhanced emission on laminate at: (—) 50 mL, (---) 25 mL, and (-·-·-) 10 mL. The reference liquid DMMP absorption spectrum (·····) is provided for comparison.

as the DMMP volume increased from 10 to 50 μL (Fig. 3). However, when DMMP is applied to laminate, the observed peaks do not match the reference peaks, likely the result of the film thickness (Fig. 3b). When DMMP is applied to SS, the observed peaks are discernably in better agreement with the reference peaks (Fig. 3a).

The band integrated absorbance,

$$A = \frac{1}{(\nu_2 - \nu_1)} \int_{\nu_1}^{\nu_2} A(\nu) d\nu \quad (2)$$

across the full spectrum, $\nu_1 = 877 \text{ cm}^{-1}$ to $\nu_2 = 1262 \text{ cm}^{-1}$, increased linearly with DMMP concentration, as shown in Fig. 4. For both the stainless steel and laminate, there was a minimal increase in absorbance at the highest DMMP volume, 50 μL , probably due to a limit on film thickness in the vertical surface preparation. Excluding the 50 μL data point, the linear fit of the stainless steel data yielded a slope of $0.00276 \pm 0.0004 \mu\text{L}^{-1}$ and $r^2 = 0.93$, and for

laminate the data yielded a slope of $0.00084 \pm 0.0002 \mu\text{L}^{-1}$ and $r^2 = 0.93$ (Fig. 4).

3.2. Imagery and classification

To assist in identifying contaminated regions, spectra were compared from the bare and contaminated surfaces using the spectral contrast angle [25]. The observed spectral absorbance, $A(\nu)$, at each frequency was compared with the NIST standard spectrum, $A_r(\nu)$, for both stainless steel and laminate surface types. The spectra were linearly correlated with correlation coefficient $r^2 = 0.84$ for the stainless steel surface. The relative amplitudes of the various vibrational features dominated the systematic differences between the reference and sample spectra. The spectral contrast angle was a convenient scalar metric for comparing these spectra and was defined as:

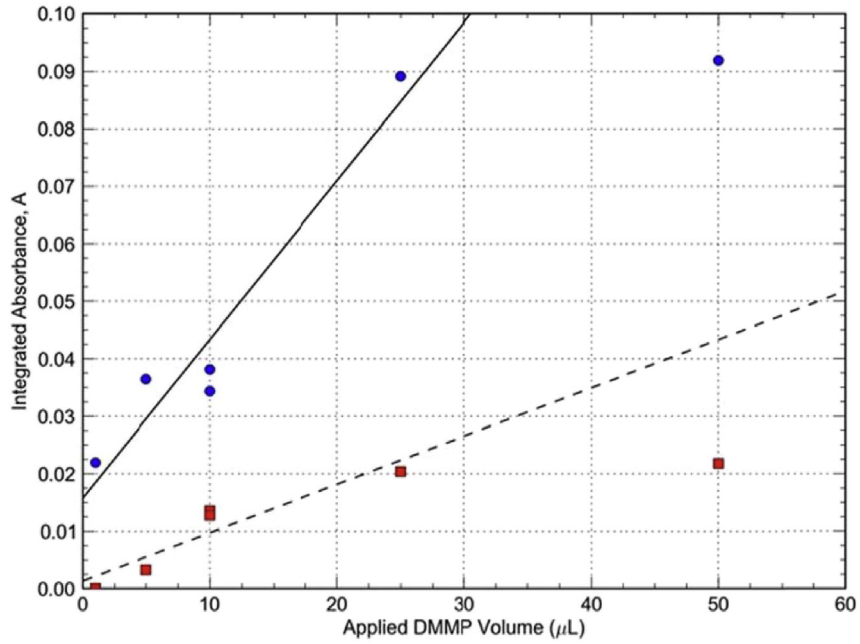


Fig. 4. Dependence of band integrated absorbance, A, on volume of applied DMMP including methanol diluted samples for: (●) stainless steel and (■) laminate, and linear fit for (—) stainless steel and (---) laminate. The 50 µL data point has been excluded from the linear fit.

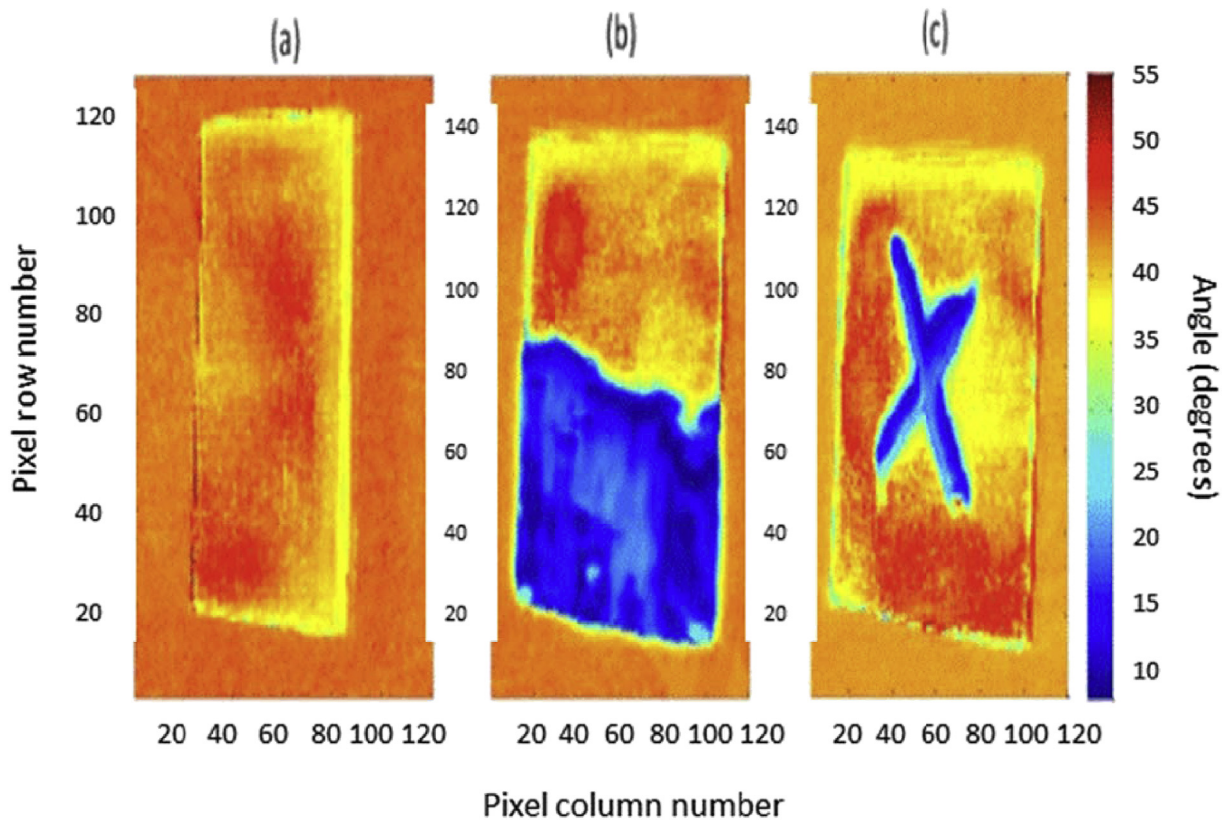


Fig. 5. Image of spectral contrast angle for: (a) bare stainless steel, (b) stainless steel with 25 µl DMMP applied to bottom half of the sample, and (c) stainless steel with 10 µl DMMP smear with X pattern. The spatial resolution is 0.8 mm/pixel.

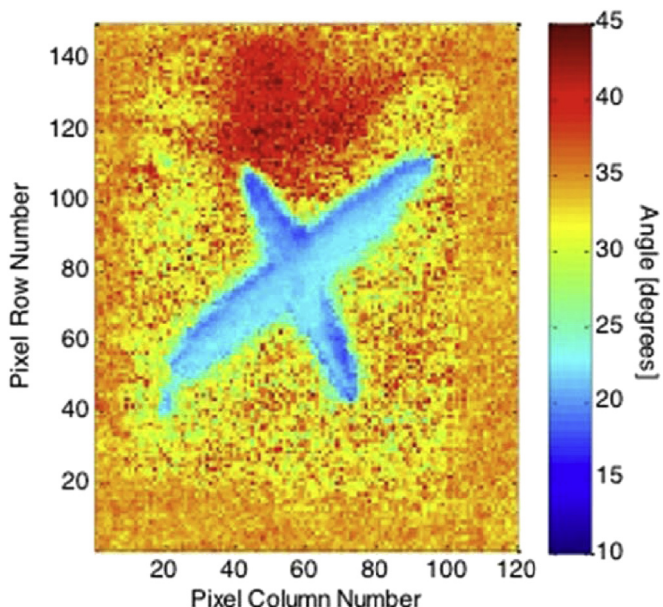


Fig. 6. Image of spectral contrast angle for 10 µL DMMP smear with X pattern on laminate.

$$\cos(\theta) = \frac{\int_{\nu_1}^{\nu_2} A(\nu)A_r(\nu)d\nu}{\left[\int_{\nu_1}^{\nu_2} A^2(\nu)d\nu \int_{\nu_1}^{\nu_2} A_r^2(\nu)d\nu \right]^{1/2}} \quad (3)$$

By considering the observed and reference spectra as two unit vectors in a high dimensional space, the angle, θ , was near zero when the spectra were similar and near 90° when the spectra did not share common features.

Fig. 5 compares a map of the spectral contrast angle, θ , for the

stainless steel samples. The reference vector was taken from the reference NIST spectra, so that small contrast angles represent contaminated areas while larger contrast angles represent segments that were not contaminated. The bare sample exhibited no contamination, with large contrast angles of 45°–55° uniformly distributed. Rectangular DMMP smears on stainless steel resulted in smaller spectral contact angles of <20° in the contaminated region and >40° in the uncontaminated region. A boundary between contaminated and uncontaminated regions was clearly identified. For stainless steel with the X-shaped smear of DMMP, the image (Fig. 5c) exhibits the same strong delineation of the contaminated region. The spatial resolution was 0.8 mm/pixel, so the transition from contaminated to bare material exhibited a sharp boundary of width of a few pixels, ~2 mm. The DMMP results on the laminate are presented in Fig. 6. In this case, the observed spectra were enhanced above the background and the enhanced emission spectra were compared to the reference spectra. The contaminated region exhibited contrast angles of <25°. There were a few randomly located, non-contiguous pixels in the bare material near this 25° boundary. The smaller, positive difference in the observed spectra led to a slight reduction in visual delineation of the contaminated region. This data does not indicate that spectral contrast angles are able to clearly indicate contaminated and uncontaminated areas on the two different tested surfaces.

3.3. Detection limits

A thorough determination of detection limits was beyond the scope of this proof-of-concept paper and requires: (1) a study of the long-term decay of the spectral signatures, (2) further evaluation of interferences from non-ideal background samples, and (3) improved pattern recognition and classification schemes. However, a few observations are possible for estimating limits of detection. First, the infrared spectra for the lower contamination levels appear to correspond well to the spectral signatures in the reference spectra (Fig. 7). The stainless steel sample, with a 1 µL smear of DMMP in methanol solution, for example, provides a clear spectral signature. The DMMP surface density calculated for a 1 µL

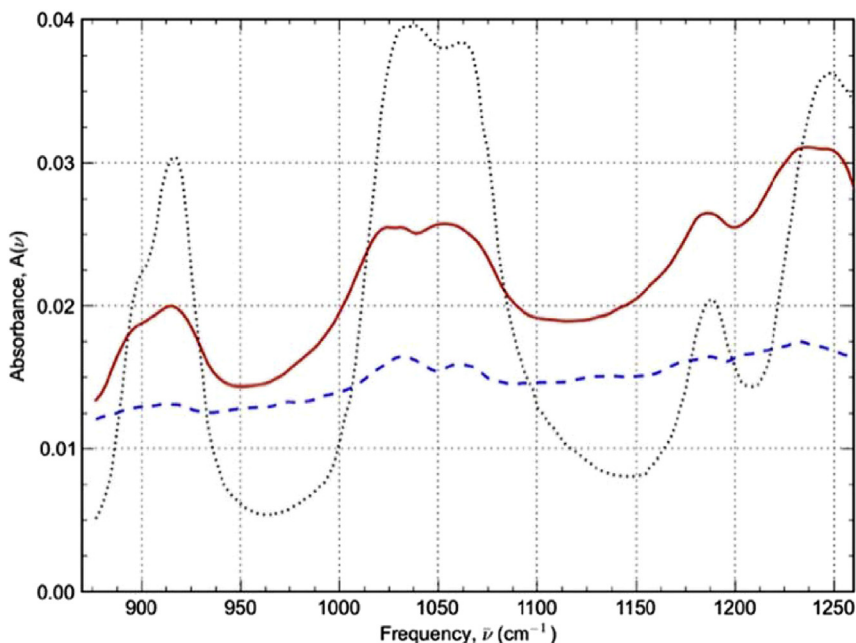


Fig. 7. Absorbance (or enhanced emission) for DMMP on (—) stainless steel at 1 µL and (---) Formica at 5 µL compared with (.....) reference spectra.

application was $22 \mu\text{g}/\text{cm}^2$, a conservative upper bound for the detection limit. Longer detector integration times, improved classification schemes, and enhanced detection strategies may significantly reduce the detection limit. The detection limit was somewhat higher for the laminate surface. When $5 \mu\text{L}$ ($110 \mu\text{g}/\text{cm}^2$) was applied to the surface, the spectral signature was weaker and primarily results from an offset in the spectral baseline. This is likely due to changes in illumination intensity. In spite of the poorer spectral signature, the map of spectral contrast angles presented in Fig. 6 visually identifies a large region with angles less than 25° where the surface was contaminated. The boundary between bare and contaminated regions still exhibits a sharp transition with a large contiguous area associated with the contamination.

The conservative upper bounds in detection limits for stainless steel and laminate (22 and $110 \mu\text{g}/\text{cm}^2$, respectively), are based on the ability to visually identify the contaminant above the baseline (background noise), in comparison to the reference spectrum for DMMP. Hence, these detection limits can be viewed as a measure of the ability to quantitatively identify the presence or absence of the compound. An estimate for the lower detection limit may be inferred from Fig. 4, based on the standard error in the slope for stainless steel ($0.0004 \mu\text{L}^{-1}$) and laminate ($0.0002 \mu\text{L}^{-1}$). Since $1 \mu\text{L}$ of DMMP was equal to $22 \mu\text{g}/\text{cm}^2$, it follows that the approximate lower detection limit was $8.8 \text{ ng}/\text{cm}^2$ and $4.4 \text{ ng}/\text{cm}^2$ for the stainless steel and laminate, respectively. Therefore, based on the data collected in the current study, the detection limit appeared to be between $8.8 \text{ ng}/\text{cm}^2 - 22 \mu\text{g}/\text{cm}^2$ for stainless steel and $4.4 \text{ ng}/\text{cm}^2$ to $110 \mu\text{g}/\text{cm}^2$ for laminate. Future work is needed to refine these approximations with larger data sets.

4. Conclusions

This research demonstrated that hyperspectral imaging can be used to detect and identify OP chemicals. This technique will most likely be applicable for other heavily used OPs as well. OPs are commonly used for applications such as controlling residential infestations, which may result in misapplication of chemicals and subsequent cleanup efforts. Furthermore, such a detector system can greatly improve field applications during an incident, such as enhanced decontamination efforts and efficacies, decreased laboratory sampling, and increased overall resiliency. Comparison of experimental and NIST reference spectra resulted in correlating absorbance bands at approximately 1275 cm^{-1} and 1050 cm^{-1} , associated with the phosphorus-oxygen double bond stretch (P=O) and phosphorus-oxygen-carbon (P–O–C) bond stretch for DMMP, respectively. The magnitude of the DMMP bands increased linearly ($r^2 = 0.93$) across the full absorbance spectrum, between $\nu_1 = 877 \text{ cm}^{-1}$ to $\nu_2 = 1262 \text{ cm}^{-1}$. The increase in absorbance was minimal at the highest DMMP volume, $50 \mu\text{L}$, perhaps due to a limit on film thickness during the vertical surface preparation. Comparisons between bare and contaminated surfaces on stainless steel using the spectral contrast angle technique indicated that the bare samples showed no sign of contamination, with large uniformly distributed contrast angles of $45^\circ - 55^\circ$. The contaminated stainless steel samples had smaller spectral contact angles of $<20^\circ$ in the contaminated region and $>40^\circ$ in the uncontaminated region. The laminate contaminated region exhibited contact angles of $<25^\circ$.

To the best of our knowledge, this is the first report to demonstrate that hyperspectral imaging can be used to detect DMMP on building materials at contamination levels relevant to real-world release scenarios. This study estimates conservative detection levels of $110 \mu\text{g}/\text{cm}^2$ (or $1100 \text{ mg}/\text{m}^2$), an order of magnitude below the $10,000 \text{ mg}/\text{m}^2$ assumed deposition rate for some chemical weapons agent munition releases [8].

These results indicate that long-wave infrared imaging can detect DMMP on stainless steel and laminate building materials. The findings establish a significant proof-of-concept with the potential to impact protocols used for stand-off detection of contaminants in indoor environments, such as residential areas and abandoned buildings. The detection method is based on the spectral signatures of the organophosphate group, thus, these results may be generally applicable to a broad group of industrial pesticides and chemical warfare agents. Further investigations involving heterogeneous surfaces and conditions that mimic the complex circumstances found in real-world field scenarios are needed to characterize this detector system and technique for a field application. More data are also needed to confirm limits of detection. Further research is required to investigate the effects of elapsed time between chemical application (or contamination) and analysis. This study imaged building materials immediately after chemical application, whereas in practical applications, field imaging would likely take place well *after* the chemical application occurred. The allowable time scales (e.g. days, months, years) for successful detection via hyperspectral imaging are not yet known. Thus, persistent chemicals are prime candidates for this research application.

Disclaimer

The views expressed in this article are those of the authors and do not reflect the official policy or position of the Air Force Institute of Technology, United States Air Force, the US Environmental Protection Agency, Department of Defense, or United States government. Mention of trade names, products, or services does not convey official EPA approval, endorsement, or recommendation.

Acknowledgements

The U.S. Environmental Protection Agency through its Office of Research and Development partially funded and collaborated in the research described here under Interagency Agreement DW-57-92390501. It has been subjected to the Agency's review and has been approved for publication. The authors thank Kelley Robinson (AFIT) and John Hixenbaugh (AFIT) for logistical assistance. We thank Dr. Daniel Felker (Analytical Chemist, AFIT) for experimental assistance.

References

- [1] H. Akbari, L. Halig, D. Schuster, A. Osunkoya, V. Master, P. Nieh, G. Chen, B. Fei, Hyperspectral imaging and quantitative analysis for prostate cancer detection, *J. Biomed. Opt.* 17 (7) (2012) 1–10.
- [2] M. Alavanja, C. Samanic, M. Dosemeji, J. Lubin, R. Tarone, C. Lynch, C. Knott, K. Thomas, J. Hoppin, J. Barker, J. Coble, D. Sandler, A. Blair, Use of agricultural pesticides and prostates cancer risk in the agricultural health study cohort, *Am. J. Epidemiol.* 157 (9) (2003) 800–814.
- [3] J. Bowen, C. Powers, A. Ratcliffe, M. Rockley, A. Hounslow, Fourier transform infrared and Raman spectra of dimethyl methylphosphonate adsorbed on montmorillonite, *Environ. Sci. Technol.* 22 (1988) 1178–1181.
- [4] R.J. Clewes, C.R. Howle, J. Guicheteau, D. Emge, K. Ruxton, G. Robertson, W. Miller, G. Malcolm, G.T. Maker, Mid-wave infrared hyperspectral imaging of unknown chemical warfare agents, in: *Proc. SPIE 8710, Chemical, Biological, Radiological, Nuclear, and Explosives (CBRNE) Sensing XIV*, 2013.
- [5] R. Das, A. Steege, S. Baron, J. Beckman, R. Harrison, Pesticide-related illness among migrant farm workers in the United States, *Int. J. Occup. Environ. Health.* 7 (4) (2001) 303–312.
- [6] J. Dich, S. Zahm, A. Hanberg, H. Adami, Pesticides and cancer, *Cancer Causes Control* 8 (3) (1997) 420–443.
- [7] E.T. Gall, T. Cheung, I. Luhung, S. Schiavon, W.W. Nazaroff, Real-time monitoring of personal exposures to carbon dioxide, *Build. Environ.* 104 (2016) 59–67.
- [8] Grotte, J. Current efforts to improve chemical challenge estimates. Chemical, Biological, Radiological, Nuclear, Survivability Conference, Baltimore, MD, 2011.
- [9] N. Kagi, S. Fujii, Y. Horiba, N. Naamiki, Y. Ohtani, H. Emi, H. Tamura, Y.S. Kim, Indoor air quality for chemical and ultrafine particle contaminants from printers, *Build. Environ.* 42 (5) (2007) 1949–1954.

- [10] M. Kim, A. Lefcourt, K. Chao, Y. Chen, I. Kim, D. Chan, Multispectral detection of fecal contamination on apples based on hyperspectral imagery. Part I. Application of visible and near-infrared reflectance imaging, *Trans. ASAE* 45 (6) (2002) 2027–2037.
- [11] Y. Kim, D. Glenn, J. Park, H. Ngugi, B. Lehman, Hyperspectral image analysis for water stress detection of apple trees, *Comput. Electron. Agr.* 77(2)(2011) 155–160.
- [12] K. Lawrence, W. Windham, B. Park, R. Buhr, A hyperspectral imaging system for identification of faecal and ingesta contamination on poultry carcasses, *J. Near Infrared Spectrosc.* 11 (4) (2003) 269–281.
- [13] S. Lee, S. Lam, H. Fai, Characterization of VOCs, ozone, and PM10 emissions from office equipment in an environmental chamber, *Build. Environ.* 36 (7) (2001) 837–842.
- [14] Makino Y., Li M., Oshita S., Kawagoe Y., Matsuoka T., Hashimoto K., Arai K. Nondestructive detection of pesticides on fruits and vegetables using UV camera. International Conference of Agricultural Engineering CIGR-AgEng2012, Valencia, Spain, 2012.
- [15] J.A. Martin, K.C. Gross, Determining index of refraction from polarimetric hyperspectral radiance measurements, *Proc. SPIE* 9613 (2015), 96130X.
- [16] P. Mehl, Y. Chen, M. Kim, D. Chan, Development of hyperspectral imaging technique for the detection of apple surface defects and contaminations, *J. Food Eng.* 61 (1) (2004) 67–81.
- [17] C. Metayer, P. Buffler, Residential exposures to pesticides and childhood leukaemia, *Radiat. Prot. Dosim.* 132 (2) (2008) 212–219.
- [18] R. Metivier, I. Leray, B. Valeur, Lead and mercury sensing by calixarene-based fluoroionophores bearing two or four dansyl fluorophores, *Chem. Eur. J.* 10 (18) (2004) 4480–4490.
- [19] NIST Standard Reference Database 69: NIST Chemistry Webbook.
- [20] H.E. Revercomb, H. Buijs, H.B. Howell, D.D. LaPorte, W.L. Smith, L. Sromovsky, Radiometric calibration of IR Fourier transform spectrometers: solution to a problem with the High-Resolution Interferometer Sounder, *Appl. Opt.* 27 (1988) 3210–3218.
- [21] T. Schneider, J. Kildeso, N.O. Breum, A two compartment model for determining the contribution of sources, surface deposition and resuspension to air and surface dust concentration levels in occupied rooms, *Build. Environ.* 34 (5) (1999) 583–595.
- [22] A.L. Smith, The coblentz society desk book of infrared spectra, *Coblentz Soc. Kirkw. MO* (1982) 1–24.
- [23] P. Usenik, M. Burmen, A. Fidler, F. Pernus, B. Likar, Near-infrared hyperspectral imaging of water evaporation dynamics for early detection of incipient caries, *J. Dent.* 42 (10) (2014) 1242–1247.
- [24] U.S. Environmental Protection Agency, in: Report to Congress on Indoor Air Quality: Volume 2, EPA/400/1-89/001C, Washington, DC, 1989.
- [25] K.X. Wan, I. Vidavsky, M.L. Gross, Comparing similar spectra: from similarity index to spectral contrast angle, *J. Am. Soc. Mass Spectrom.* 13 (2002) 85–88.
- [26] C.J. Weschler, Changes in indoor pollutants since the 1950s, *Atmos. Environ.* 43 (1) (2009) 153–169.
- [27] A. Zawadzki, D. Shrestha, B. He, Biodiesel blend level detection using ultraviolet absorption spectra, *Trans. ASABE* 50 (4) (2007) 1349–1353.
- [28] Y. Zhang, Z. Cheng, A. Li, S. Feng, Mid-infrared absorption spectra of dimethyl methylphosphonate as molecular simulant of nerve agents, *Chin. Opt. Lett.* 4 (2006) 608–610.
- [29] H. Zhang, J. Xie, H. Yoshino, U. Yanagi, K. Hasegawa, N. Kagi, Z. Lian, Thermal and environmental conditions in Shanghai households: risk factors for childhood health, *Build. Environ.* 104 (2016) 35–46.
- [30] J. Wahl, H. Colburn, Extraction of chemical impurities for forensic investigations: a case study for indoor releases of a sarin surrogate, *Build. Environ.* 45 (5) (2010) 1339–1345.